Mapping Surface Soil Freeze-Thaw Cycles in China Based on SMMR and SSM/I Brightness Temperatures from 1978 to 2008

Authors: Jin, Rui, Zhang, Tingjun, Li, Xin, Yang, Xingguo, and Ran, Youhua

Source: Arctic, Antarctic, and Alpine Research, 47(2) : 213-229

Published By: Institute of Arctic and Alpine Research (INSTAAR), University of Colorado

URL: https://doi.org/10.1657/AAAR00C-13-304

Arctic, Antarctic, and Alpine Research, Vol. 47, No. 2, 2015, pp. 213–229

Mapping surface soil freeze-thaw cycles in China based on SMMR and SSM/I brightness temperatures from 1978 to 2008

Rui Jin[1,2]
Tingjun Zhang[3,5]
Xin Li[1,2]
Xingguo Yang[4] *and*
Youhua Ran[1]

[1]Cold and Arid Regions Environmental and Engineering Research Institute, Chinese Academy of Sciences, 320 West Donggang Road, Lanzhou, 730000, China
[2]Chinese Academy of Sciences Center for Excellence in Tibetan Plateau Earth Sciences, Beijing 100101, China
[3]MOE Key Laboratory of West China's Environmental System, College of Earth and Environmental Sciences, Lanzhou University, 222 South Tianshui Road, Lanzhou, Gansu, 730000, China
[4]Meteorology Bureau of Gansu Province, 2070 Donggang East Road, Lanzhou, Gansu, 730020, China
[5]Corresponding author: tjzhang@lzu.edu.cn

Abstract

This paper aims to provide a long time-series data set documenting the surface soil freeze-thaw cycles in China over a period of more than 30 years. The remote sensing data are from the daily brightness temperatures recorded by the Scanning Multichannel Microwave Radiometer (SMMR, 1978–1987) and Special Sensor Microwave Imager (SSM/I, 1987–2008), which have a 25 km spatial resolution. The classification method used to identify the surface soil freeze-thaw states is a dual-indices algorithm based on the 37 GHz vertical polarization brightness temperature and spectral gradient between the 37 GHz and 18/19 GHz brightness temperatures. This algorithm has been recalibrated for SMMR and SSM/I using the in situ daily minimal ground surface temperatures observed at 77 meteorological stations covering the dominant land surface types of China. The daily classifications of surface soil freeze-thaw states were validated by observations from an additional 273 meteorological stations. The classification accuracy of the frozen and thawed soils as well as the total accuracy exceed 80%. Based on this data set, we analyzed the seasonal and interannual variations across the areal extent and timing of surface soil freezing, trend of the onset date of surface soil freezing and thawing, and duration of surface soil thawing in China. The results showed that the maximum frozen extent during 1978–1987 was 6.93×10^6 km^2 or 72.8% of the area, and it generally occurred in late December and January. The minimum frozen extent was 0.26×10^6 km^2 or 3.0% of the area, and it occurred in late July and August. The first day of soil freezing occurred between September and November, whereas the first day of soil thawing occurred between March and May. The trend analysis demonstrated that from 1978 to 2008, the onset date of surface freezing was postponed by 19.6 ± 14.6 days, whereas the onset of surface thawing was advanced by –19.0 ± 9.4 days, and the thawing period was prolonged by 34.3 ± 16.5 days. These trends revealed a pattern of earlier thawing, later freezing, and longer growing seasons because of climate warming, especially in the seasonally frozen ground and permafrost regions with high ground temperatures.

DOI: http://dx.doi.org/10.1657/AAAR00C-13-304

Introduction

Approximately 57% of land surfaces experience freezing and thawing processes annually in the northern hemisphere (Zhang et al., 2003). These processes have extensive and profound influences on the energy, water, and mass exchanges between the atmosphere and land surface and also affect surface runoff, plant growth, and engineering stability.

The transitions in the surface soil between frozen and thawed states initiate the wintertime dormancy and summertime activity of the terrestrial processes; these transitions can also be characterized as a switch of the hydrological cycle and ecosystem activity (McDonald and Kimball, 2005). When the soil freezes in autumn, the liquid soil water largely becomes solid ice, resulting in a decrease in soil heat capacity and increase in soil thermal conductivity. Furthermore, the presence of a thin frozen soil layer near the ground surface dramatically decouples the water exchange between the atmospheric boundary layer and deeper soil layers (Zhang et al., 2003). When air temperatures increase above 0 °C during the early spring, the frozen land surface starts to thaw. Because of the substantial latent heat of fusion used in the snow melting process, the underlying surface soil remains frozen and restrains the snowmelt water from infiltrating the soil, resulting in an accelerated and enhanced generation of surface runoffs. As the frozen surface soil thaws with continued warming, the ecosystem becomes active (Goulden et al., 1998; Jarvis and Linder, 2000; Black et al., 2000). Therefore, the information on surface soil freeze-thaw states is important for determining the rates of soil respiration, plant photosynthesis, growing season, net primary production, and winter irrigation of cropland (Running et al., 1999).

The spatial distribution of frozen ground surfaces varies substantially on daily, seasonal, and annual scales (Zhang et al., 2003). The timing at which the surface soil begins to freeze and thaw, and duration and total number of days at which the surface soil remains frozen also change substantially, especially as the climate changes. An overall understanding of the spatio-temporal dynamics of surface soil freeze-thaw cycle is important for research on climate change, hydrology, ecology, and agriculture.

In situ observations can provide detailed information on the active layer in areas affected by frozen ground at the point scale, such as soil temperature and moisture profiles. However, it is difficult to represent the frozen ground distribution, and in situ observations are usually used to calibrate and validate the model simulations and remote sensing retrievals.

1523-0430/03 $7.00

Remote sensing technology, such as thermal infrared and microwave remote sensors (Zhang et al., 2001), possesses sophisticated capabilities to monitor global and regional surface soil freeze-thaw states. Thermal infrared remote sensors can measure surface temperatures with resolutions of 10–1000 m, which are sufficient to determine the surface soil freeze-thaw states. Examples of such sensors include the Thematic Mapper (TM), Advanced Spaceborne Thermal Emission and Reflection Radiometer (ASTER), and MODerate-resolution Imaging Spectroradiometer (MODIS). However, land surface radiative temperatures retrieved from these sensors are severely influenced by water vapor, aerosol, and cloud cover in the atmosphere. Furthermore, the surface soil freeze-thaw states are difficult to identify when the ground surface is covered by canopy. Microwave remote sensing can work under most weather conditions and penetrate the surface covering to detect the underlying soil status at 1–10 cm depth. Microwave signals are sensitive to the liquid soil water content because the dielectric constant of liquid water is much greater than that of soil particles, ice, and other natural materials. The dielectric constant of a mixed material mainly depends on the dielectric property and volumetric fraction of each constituent. For example, the frozen soil comprises soil particles, air in voids, and water in liquid and solid states. When the soil freezes and the liquid soil water becomes ice, the soil dielectric constant decreases substantially. The sharp change in soil dielectric properties resulting from the phase change of soil moisture makes it beneficial to distinguish the surface soil freeze-thaw states using microwave remote sensors. Both active (i.e., radar and scatterometer) and passive microwave remote sensors are widely used for monitoring surface freeze-thaw states (Zuerndorfer et al., 1990; Zuerndorfer and England, 1992; Judge et al., 1997; Zhang and Armstrong, 2001; Smith et al., 2004; Zhang et al., 2001; Jin et al., 2009), detecting early spring thawing events (Bartsch et al., 2007; Wismann, 2000; Kimball et al., 2004a), and studying plant growing seasons (Kimball et al., 2004b; Frolking et al., 1999).

The main advantage of active microwave remote sensing is that there is a monotonic change of the backscattering coefficient along with soil liquid water content, whereas the soil temperature has little influence on backscattering. However, the backscattering signal is also sensitive to the geometric features of land surface, including the canopy structure and surface roughness. Additionally, the active radar has a higher spatial resolution in the range of tens of meters but a longer revisiting time interval, which may cause a deficiency in capturing the surface soil freeze-thaw transitions in spring and autumn. The scatterometer is another type of active microwave sensor with a twice per day or better revisiting frequency; however, it has a coarse spatial resolution of approximately 25–50 km. Furthermore, both radars and scatterometers have a relatively short period of data archiving, making them inappropriate for analyzing the response of surface freeze-thaw cycles to climate change.

The launches of Scanning Multichannel Microwave Radiometer (SMMR, 1978–1987), Special Sensor Microwave Imager (SSM/I, 1987–present), and Advanced Microwave Scanning Radiometer–EOS (AMSR-E, 2002–2011) have resulted in continuous time-series records of global passive microwave brightness temperatures for more than 30 years. Thus, these passive microwave brightness temperatures are suitable for monitoring surface freeze-thaw cycles over a long period and from regional to global scale.

There are three major types of surface freeze-thaw state classification algorithms that use passive microwave brightness temperatures: dual-indices algorithm (Zuerndorfer et al., 1990, Zuerndorfer and England, 1992; Judge et al., 1997; Zhang et al., 2003), change detection algorithm (Smith et al., 2004), and decision tree algorithm (Jin et al., 2009). All of these algorithms are based on the special microwave radiative characteristics associated with frozen soil, such as the lower soil temperature, higher surface emissivity, and volume scattering effect.

The dual-indices algorithm, which uses $T_{B,37V}$ and a spectral gradient (SG), has been widely used since the 1990s. The dual-indices algorithm, which applies unified calibrated thresholds throughout the research regions, can be easily implemented in operational mode. However, this algorithm does not consider the diversity of land surface types, which limits improvements to its classification accuracy. Furthermore, the mean daily air temperature (Zuerndorfer et al., 1990; Zuerndorfer and England, 1992; Zhang et al., 2003) and soil temperature generally adopted for the algorithm calibration cannot accurately represent the true surface soil freeze-thaw states when the radiometers pass over.

The change detection algorithm, which is based on the time-series of microwave observations, originated from active microwave remote sensing. Smith et al. (2004) developed a new change detection algorithm applicable to passive microwave sensors by using the value of $(T_{B,37}\text{-}T_{B,18/19})$ to identify the plateau that indicates the transition from frozen to thawed states of soil. However, the gradual changing of soil temperature during the freezing process and asynchronous development of surface freezing in a coarse passive microwave pixel may result in the inability of algorithm to recognize abrupt changes in spectral signals.

The decision-tree algorithm for SSM/I is developed to eliminate the influence of other surface scatterers, such as desert and precipitation, to improve classification accuracy (Jin et al., 2009). This algorithm introduces the scattering index, polarization difference at 19 GHz, and $T_{B,37V}$ as the classification criteria. However, there are no high-frequency observations at 85 GHz for the SMMR, making it difficult to use the decision-tree algorithm with SMMR radiometers.

In this study, the dual-indices algorithm was calibrated using the in situ daily minimal ground surface temperature for each dominant land surface type and was used to produce a long time-series data set of surface soil freeze-thaw cycles for 30 years by combining the daily SMMR and SSM/I brightness temperatures. The seasonal and interannual variations in the areal extent and timing of soil freezing, trend of the onset date of surface freezing and thawing, and duration of surface thawing are analyzed throughout China to understand the response of frozen ground to climate change.

Data Sources

In this study, the data sets used to calibrate and validate the surface soil freeze-thaw classification algorithm included the passive microwave brightness temperatures, in situ soil temperatures, map of land use, and a digital elevation model (DEM). The following sections describe these data in detail.

PASSIVE MICROWAVE BRIGHTNESS TEMPERATURE

The daily brightness temperatures recorded by the SMMR (31 October 1978–3 August 1987) and SSM/I (4 August 1987–27 March 2008) were provided by the National Snow and Ice Data Center (NSIDC) in the Equal-Area Scalable Earth Grid (EASE-Grid) format (Armstrong et al., 2008). The NSIDC EASE-Grid passive microwave data sets have a spatial resolution of 25 km and descending and ascending observations separated by the overpass time of radiometers. The detailed instrument parameters for both

TABLE 1

Parameters of SMMR and SSM/I.

Parameters	SMMR (Nimbus-7)	SSM/I (DMSP)
Frequency (GHz)	6.6, 10.7, 18.0, 21.0, 37.0	19.35, 22.3, 37.0, 85.5
Orbit height (km)	955	860
Antenna size (m)	0.79	0.6
Incidence angle (°)	50.3	53.1
Swath (km)	780	1400
Service period	1978–1987	1987–present
Overpass time	12:00/24:00	06:00/18:00

radiometers are shown in Table 1. The $T_{B,18V}$ and $T_{B,37V}$ for the SMMR and $T_{B,19V}$ and $T_{B,37V}$ for the SSM/I were used for the dual-indices algorithm to maintain consistency. Judge et al. (1997) concluded that the O_2, H_2O, and cloud corrections had little influence on the dual-indices algorithm; therefore, atmospheric corrections were not conducted in data processing. The slight differences in incident angle and frequency between the SMMR and SSM/I data were also considered to have little influence on this classification algorithm (Picard and Fily, 2006).

However, there is a large difference in the overpass time of the two radiometers, which is a major concern for obtaining a long time-series data set of surface soil freeze-thaw cycles. The SMMR overpasses at approximately 12:00 and 24:00 local time, and the SSM/I overpasses at approximately 06:00 and 18:00 local time. A comparison of the SMMR and SSM/I brightness temperatures during their overlapping period shows that the SSM/I brightness temperatures are systematically higher than the SMMR measurements, with a magnitude of 4–9 K (Derksen and Walker, 2003). To eliminate the classification uncertainty of surface soil freeze-thaw states that result from the different overpass times of SMMR and SSM/I, we calibrated both indices using the same in situ observation variable. Furthermore, to avoid the extinction influence of wet snow, cold-overpass observations at midnight or in the early morning are recommended to capture the daily surface soil freeze-thaw cycles; these observations include the SMMR ascending T_B at 24:00, F8-SSM/I ascending T_B at 6:00, F11-SSM/I descending T_B at 6:00, and F13-SSM/I descending T_B at 6:00. Because the liquid water on the surface of wet snow has a strong absorption extinction for microwave energy, it can obscure the microwave radiance from the underlying soil in frozen or thawed states.

To eliminate the abnormal brightness temperatures resulting from radiometer instability and atmospheric influences, quality controls of data are implemented. If a datum satisfies any one of the following criteria, it is discarded: (1) T_B at any channel is equal to zero; (2) the difference in T_B between the vertical and horizontal polarization at any frequency is less than zero; and (3) T_B is beyond the bounds of the mean ± 2 × standard deviation of T_B at any channel.

CMA SOIL TEMPERATURE

The daily mean and minimum ground surface temperatures for 1978 through 2006 have been collected from stations administered by the China Meteorological Administration (CMA). The daily mean ground surface temperature is the average of the 0 cm soil temperature measured at 02:00, 08:00, 14:00, and 20:00 Beijing Standard Time. The daily minimal ground surface temperature is recorded with a minimum thermometer. The land surfaces of all of the CMA stations have flat bare soil or grass that is less than 20 cm high. This study uses ground surface temperatures from 77 CMA stations for algorithm calibration and another 273 CMA stations for validation. These CMA stations are mainly distributed in permafrost and seasonally frozen ground regions (see Fig. 1).

The hourly ground surface temperatures from 1 August 2002 to 1 April 2003, are provided by the automatic meteorological stations supported by Coordinated Enhanced Observing Period (CEOP) and used to explore the relationship between the ground surface temperature at radiometer overpass times and CMA daily surface temperature. These relationships are then adopted to calibrate the dual-indices algorithm.

LAND USE MAP

The vector land use map at 1:100,000 scale is generated based on the Landsat/TM and CBERS-1 (China-Brazil Earth Resources Satellite-1) images (Liu et al., 2003). The random sampling survey and validation in the field with a 70,000 km transect that includes 13,300 quadrats demonstrate that the interpretation accuracy is approximately 92.9%. This 1:100,000 land use map is then converted into the NSIDC EASE-Grid format by the area-weighted resample method (see Fig. 2). The areal fraction of water for each EASE-Grid pixel is also calculated, and pixels with water fractions greater than 40% are eliminated from the classification (Basist et al., 1998).

DEM

The EASE-Grid 25 km DEM is produced by reprojecting and resampling the 500 m resolution DEM provided by the Environmental and Ecological Science Data Center for West China (http://westdc.westgis.ac.cn). The elevation increases from less than 1000 m in southern and eastern China to approximately 3000 m in northwestern China, and it is higher than 3500 m on the Qinghai-Tibetan Plateau (see Fig. 1). In addition to latitude, elevation is another major factor controlling the distribution of frozen ground in China, especially on the Qinghai-Tibetan Plateau and in mountainous regions (Zhou et al., 2000).

Classification Algorithm for Surface Soil Freeze-Thaw State

To produce a long time-series data set of surface soil freeze-thaw states, the $T_{B,18V}$ and $T_{B,37V}$ of SMMR and $T_{B,19V}$ and $T_{B,37V}$ of SSM/I are selected for use in the dual-indices algorithm (Equations 1 and 2). To further improve the classification accuracy, thresholds are calibrated for each land surface type using the in situ ground surface temperature observations throughout China.

$$T_{B,37v} < T_{cutoff} \tag{1}$$

$$(SP = T_{B,37v} - T_{B,18/19v}) < SP_{cutoff} \tag{2}$$

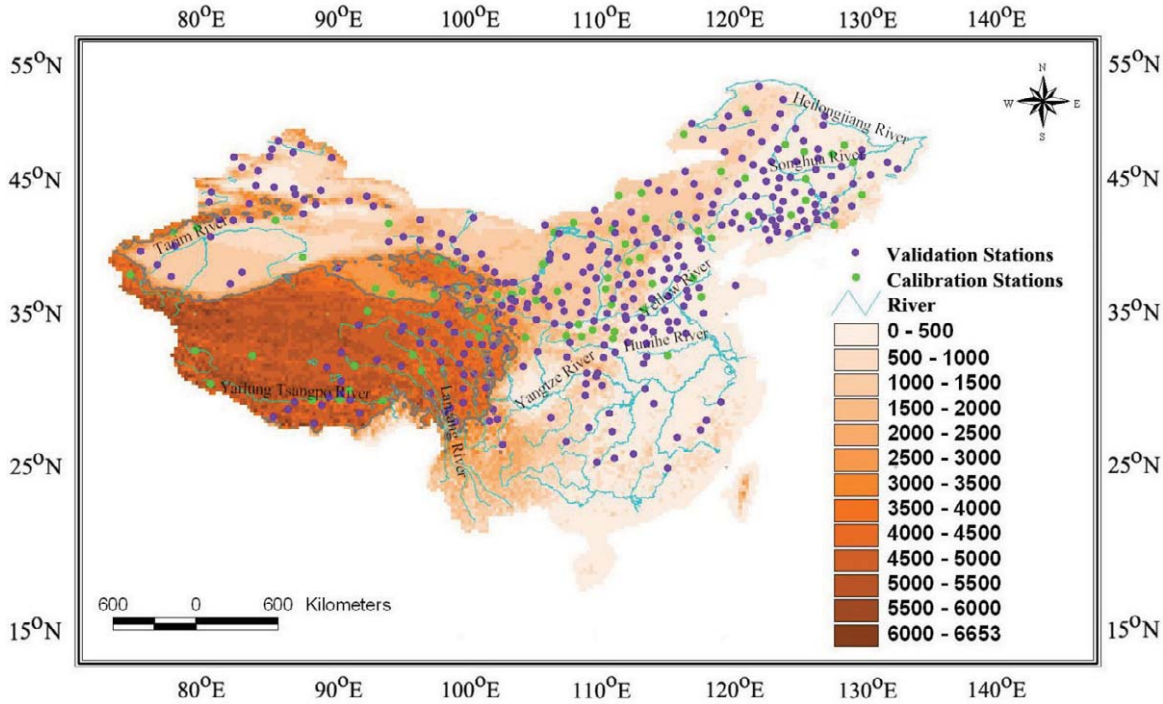

FIGURE 1. Distribution of CMA stations for algorithm calibration (green points) and validation (purple points) in China. The background is EASE-Grid DEM with 3500 m contours (gray lines).

ALGORITHM CALIBRATION

Table 2 shows the definition, area fraction, and altitude range of each land surface type. The dominant land surface types in China include grassland (with an area fraction of 33.3%), forest (24.8%), cropland (20.2%), unusable land (13.9%), desert (5.7%), and water body (2.1%). Each type has different microwave radiative characteristics because of the dielectric and geometry properties. For

TABLE 2

Area and altitude range of land use types in China.

Land surface type	Area (km^2)	Fraction (%)	Altitude (m)	Definition
Irrigated cropland	488,880	5.13	<2000	Dependent on the artificial irrigation system
Non-irrigated cropland	1,438,364	15.09	<3000	Dependent on precipitation
Dense forest	1,445,904	15.17	<3600	Woodland, crown density >30%
Sparse forest	531,610	5.58	<3600	Woodland, crown density of 10–30%
Shrub land	382,684	4.02	<3600	Shrub, crown density >40% and height<2 m
High-coverage grassland	1,242,309	13.04	<6000	Coverage >50%
Medium-coverage grassland	1,200,207	12.59	<6000	Coverage of 20–50%
Low-coverage grassland	731,435	7.68	<6000	Coverage of 5–20%
Water body	197,311	2.07		River and channel, lake, reservoir and pond, glacier and firn, overflow land
Desert	542,921	5.70		Stony and alpine desert with a vegetation coverage <5%
Unusable land	1,327,770	13.93		Gobi, saline-alkali land, bare soil, bare rock
Total	9,529,395	100.00		

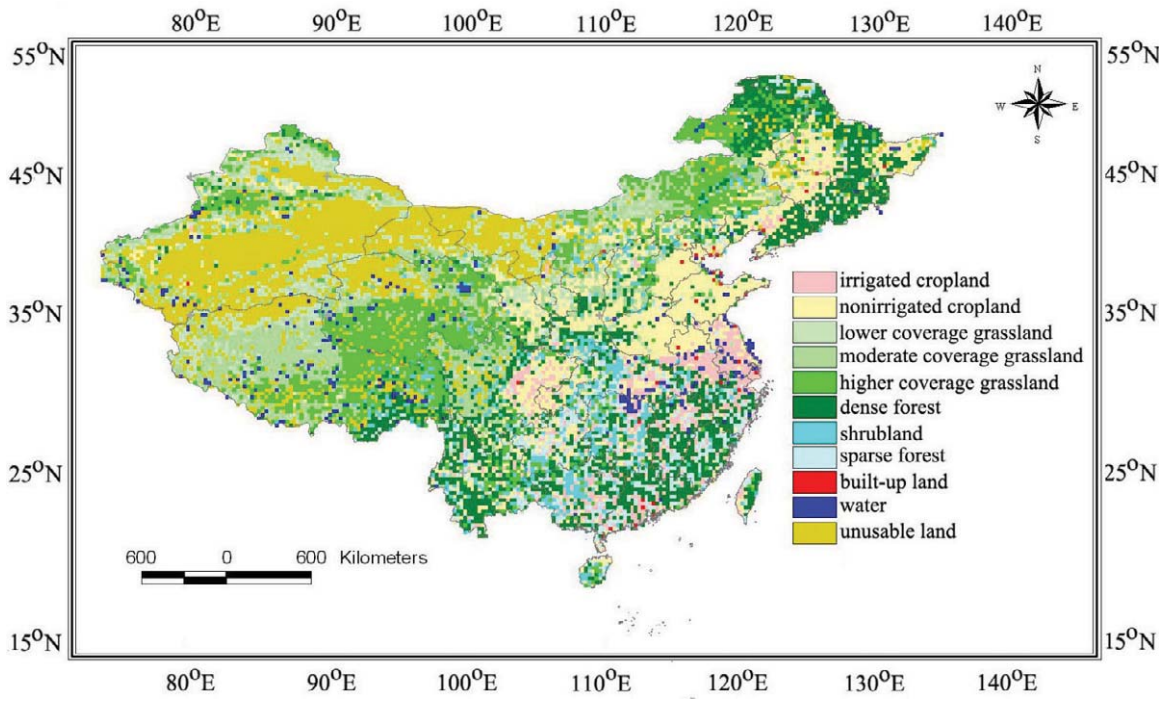

FIGURE 2. EASE-Grid land use types of China.

example, for soils with similar water content, microwave brightness temperatures may vary with the soil texture, vegetation type, and coverage. However, previous studies applied unified thresholds across the entire study region without considering the diversity of land surface types. We attempt to improve the overall accuracy of the surface soil freeze-thaw classification algorithm by calibrating the threshold for each land surface type. Furthermore, to account for the wide altitude range (from 0 m to 6000 m) of grassland, an elevation of 3500 m is used to separate the high-, medium-, and low-coverage grassland into two subtypes. The grassland subtypes with an elevation of >3500 m are mainly distributed on the Qinghai-Tibetan Plateau, where frozen ground is widely distributed and surface soil freeze-thaw cycles occur frequently.

We have selected calibration stations from the CMA stations for each land surface type according to the land surface similarity between the pixel where the station is located and surrounding pixels based on the EASE-Grid land use map. The 77 stations surrounded by grids $\geq 3 \times 3$ with the same land surface type have been selected to calibrate the dual-indices algorithm (see Fig. 1).

The daily ground surface soil temperatures or air temperatures are used directly to calibrate the classification algorithm in the previous research. However, these temperatures do not represent the actual soil freeze-thaw states at the time of the radiometer overpass. In this research, we attempt to calibrate the algorithm using daily ground surface temperatures projected at the hour of satellite overpass.

The regression relationship between the CMA daily ground surface temperature and surface temperature at the hour of satellite overpass is exploited. Because of the limited availability of hourly observations, we only use the CEOP surface temperature observations on the Qinghai-Tibetan Plateau during the period from 1 October 2002 to 30 September 2003. The daily average surface temperature ($\boldsymbol{T}_{s\_ave}$) and daily minimum surface temperature ($\boldsymbol{T}_{s\_min}$) are calculated from the hourly observations. The surface temperatures at 24:00 and 06:00 hours are synchronized with the SMMR ascending data and F11-SSM/I descending data and regarded as $\boldsymbol{T}_{s\_smmr}$ and $\boldsymbol{T}_{s\_ssmi}$, respectively. The comparison of these observations at the Gaize Station (32.3°N, 84.5°E, 4416 m, grassland) illustrates that the daily surface temperatures are clearly correlated with $\boldsymbol{T}_{s\_smmr}$ and $\boldsymbol{T}_{s\_ssmi}$, and $\boldsymbol{T}_{s\_ave} > \boldsymbol{T}_{s\_smmr} > \boldsymbol{T}_{s\_ssmi} > \boldsymbol{T}_{s\_min}$ (see Fig. 3). Because the SSM/I overpass occurs at 06:00, which is approximately sunrise, the $\boldsymbol{T}_{s\_ssmi}$ is closer to the $\boldsymbol{T}_{s\_min}$ than the $\boldsymbol{T}_{s\_smmr}$. Least-squares linear regressions are conducted between the daily surface temperature ($\boldsymbol{T}_{s\_ave}$ or $\boldsymbol{T}_{s\_min}$) and surface temperatures at the hour of radiometer overpass ($\boldsymbol{T}_{s\_ssmi}$ or $\boldsymbol{T}_{s\_smmr}$). The regression lines and 1:1 lines are shown in Figure 4 for both SMMR and SSM/I. Both figures indicate that the determination coefficient (R^2) of the regression relationship between $\boldsymbol{T}_{s\_min}$ and $\boldsymbol{T}_{s\_ssmi}/\boldsymbol{T}_{s\_smmr}$ is greater than the R^2 between $\boldsymbol{T}_{s\_ave}$ and $\boldsymbol{T}_{s\_ssmi}/\boldsymbol{T}_{s\_smmr}$. Therefore, the daily minimum surface temperature ($\boldsymbol{T}_{s\_min}$) is an optimal variable to calibrate the dual-indices algorithm. According to the regression equations in Figure 4, when the surface temperatures at the hour of radiometer overpass equal the soil freezing point (0 °C), the corresponding daily minimum surface temperatures should be –4.02 °C for the SMMR data and –1.07 °C for the SSM/I data. These temperatures are adopted as thresholds to indicate the actual surface soil freeze-thaw states of training samples from calibration sites. However, the application of these thresholds to other land surface types should be evaluated when the data are available.

The mean (gray dot), standard deviation (transverse bar), and double standard deviation (top and bottom of vertical bar) of the $T_{B,37V}$ are calculated for the frozen (blue) and thawed (red) training samples of each land surface type. Figure 5 demonstrates that the $T_{B,37V}$ of frozen soil is clearly lower than that of thawed soil, although there is a small overlap. The thresholds of $T_{B,37V}$ are de-

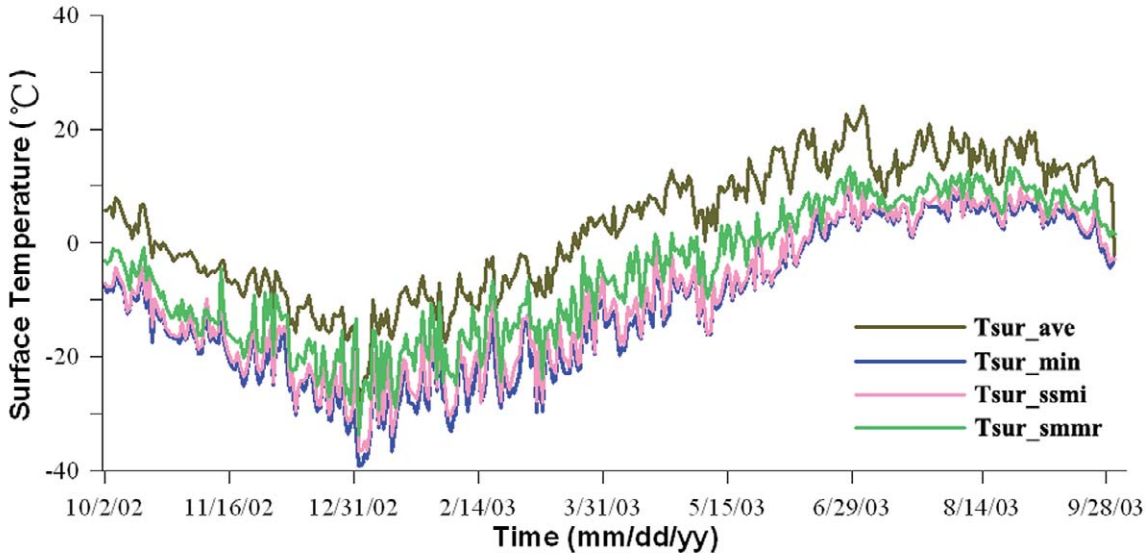

FIGURE 3. Time series of daily average surface temperature (T_{sur_ave}), daily minimum surface temperature (T_{sur_min}), surface temperature from the SSM/I overpass at 06:00 local time (T_{sur_ssmi}), and surface temperature from the SMMR overpass at 24:00 local time (T_{sur_smmr}). Dates are given as mm/dd/yy.

termined at the points where they separate the frozen and thawed training samples with the highest accuracy. The SG of frozen soil is also less than that of thawed soil, and the threshold of SG is set to zero because of the volume-scattering effect of frozen soil. A pixel is regarded as being in a frozen state if both $T_{B,37V}$ and SG are less than the thresholds; otherwise, the pixel is classified as being in the thawed state.

Further considerations are made to improve the classification accuracy. First, pixels with a water fraction greater than 40% are excluded, which includes mixed pixels near the coast and large lakes. The desert in cold weather may be misclassified as frozen soil because it has the same volume-scattering darkening effect as frozen soil. Thus, we mask out all of the desert pixels based on the EASE-Grid land use map. Second, precipitation may also be confused with frozen soil because it also exhibits strong volume scattering. Precipitation is usually identified by the 22 GHz and 85 GHz T_B (Grody, 1991; Fiore and Grody, 1992). However, this method cannot be applied to distinguish precipitation using the SMMR data because of the lack of high-frequency observations. Third, the monthly impossible-frozen-extent masks are produced using the daily minimum surface temperature observed at the 848 CMA stations from 1977 to 2006. The inverse distance-weighted method is adopted to interpolate the CMA in situ data into the EASE-Grid format. If the minimum of the monthly average of the daily minimum surface temperature during the 30 years is greater than 0 °C, this region is regarded as having never been frozen. Thus, the pixels in this region should be classified as being in a thawed state, although the values of $T_{B,37V}$ and SG are lower than the thresholds.

ALGORITHM VALIDATION

To evaluate the accuracy of this classification algorithm, we use the following assessment index (Zhang et al., 2003): (1) $F_{\surd}$, the number of pixels that are correctly classified as being in the frozen state; (2) $F_{\times}$, the number of pixels that are wrongly classified as being in the frozen state; (3) $T_{\surd}$, the number of pixels that are correctly classified as being in the thawed state; and (4) $T_{\times}$, the number of pixels that are wrongly classified as being in the thawed state.

We then perform the following calculations using the above-defined variables to estimate the classification accuracy for frozen soil, thawed soil, and the total:

$$\text{classification accuracy of frozen soil} = F_{\surd} / (F_{\surd} + T_{\times}), \quad (3)$$

$$\text{classification accuracy of thawed soil} = T_{\surd} / (T_{\surd} + F_{\times}), \quad (4)$$

$$\text{total classification accuracy} = (F_{\surd} + T_{\surd}) / (F_{\surd} + F_{\times} + T_{\surd} + T_{\times}). \quad (5)$$

The ground truth is composed of the daily minimum ground surface temperatures from another 273 CMA stations (see Fig. 1) from 31 October 1978 through 31 December 2006. Overall, the algorithm can achieve classification accuracies of 88.3% for frozen soil when using the SMMR and 84.0% when using the SSM/I, and classification accuracies of 86.2% for thawed soil when using the SMMR and 92.4% when using the SSM/I. The total classification accuracy is approximately 87.4% for SMMR and 88.7% for SSM/I (see Table 3).

Results

Based on the recalibrated dual-indices algorithm, the daily surface soil freeze-thaw states have been obtained for the period from 1978 to 2008. Because the SMMR observations are collected on alternate days and because of accidentally missing observations from both the SMMR and SSM/I, the surface soil freeze-thaw states on days with no T_B observations are replaced with the most adjacent classification result. Then, moving window compositing

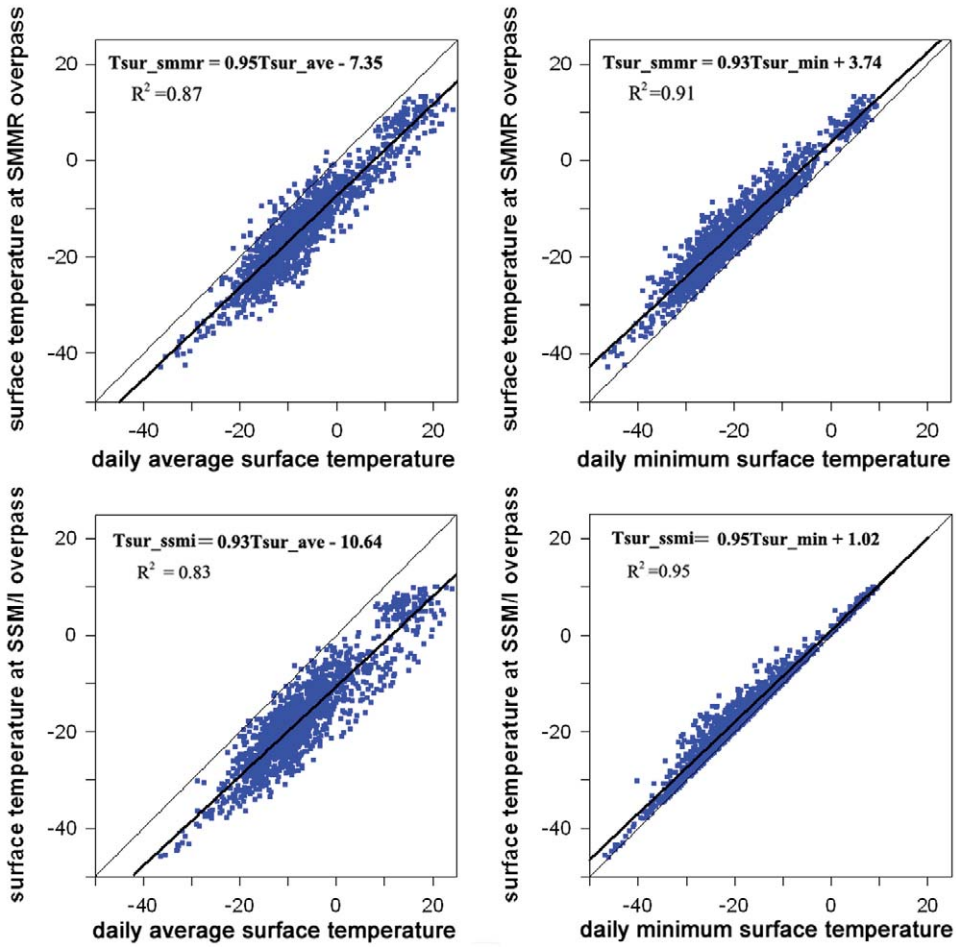

FIGURE 4. Linear regression between daily surface temperatures and T_{sur} at the time of radiometer overpass.

with a window size of 7 days (day No. 1–No. 7, day No. 2–No. 8, and so forth) is conducted for the frozen pixels to fill in the gaps between the neighboring swatches to achieve full coverage over China. The composited classification results are used to analyze the seasonal and interannual variations in the extent and timing of soil freezing and thawing. The first day of an analysis year is set as 1 July, and June 31 of the following year is set as the last day of an analysis year.

PROBABILITY OF SOIL FREEZING

The probability of soil freezing is obtained by dividing the total number of frozen days by the total number of days during the study period (1978–2008). Figure 6, part a, shows that primarily on the northwestern Qinghai-Tibetan Plateau this probability is above 80%, and in southern China (below 35°N), the probability is less than 20%, which is mainly because of the exceptionally cold current. In northern China (above 35°N), the probability of soil freezing is 30%–50%, and in northeastern China, it is approximately 40%–80%. The probability of soil freezing increases gradually with altitude (see Fig. 6, part b) rather than with latitude because the mountain permafrost and seasonally frozen ground are widely distributed on the Tibetan Plateau and cover 26°N–36°N (see Fig. 6, part c).

SEASONAL AND INTERANNUAL VARIATIONS IN THE FROZEN EXTENT

The seasonally frozen extent varies significantly. Figure 7 shows the frozen extent on the 15th day of each month from July 2001 to June 2002. The maximum and minimum frozen extents are approximately 6.48×10^6 km^2 and 1.18×10^6 km^2, respectively; account for 68.2% and 12.4% areal fraction of the total Chinese land; and occurred in December 2001 and July 2002, respectively. The northwestern Qinghai-Tibetan Plateau and northeastern China begin to freeze in September and are the earliest regions to start freezing. The frozen extent then progresses to northern China during October and progresses southward from November to January of the following year. From February, the frozen extent decreases rapidly and continuously draws back to northern China until June. The Qinghai-Tibetan Plateau does not completely thaw until the end of June because of its high altitude. The southern limit of the frozen extent is near the Huaihe River.

The interannual variations of frozen extent and its areal fraction are analyzed for the period from 1978 to 2008 (see Fig. 8). The frozen extent variation and maximum frozen extent are relatively stable. The average maximum frozen extent for the 30-year period is 6.93×10^6 km^2 or 72.8%, and it occurs in late December and January, whereas the average minimum frozen extent is 0.26×10^6 km^2 or 3.0%, and it occurs in late July and August. The warmest winter

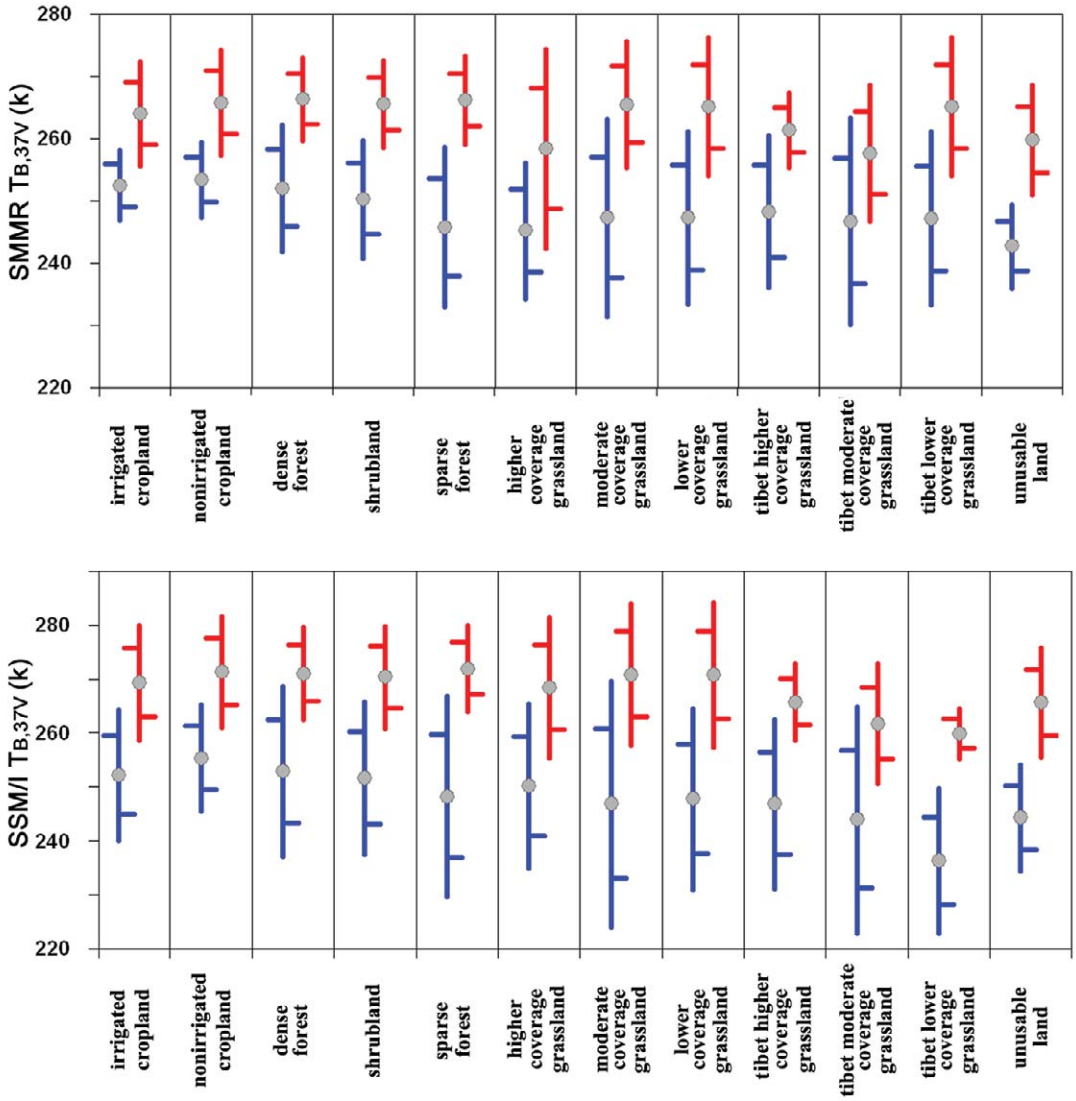

FIGURE 5. Mean, standard deviation, and double standard deviations of SMMR $T_{B,37V}$ (top) and SSM/I $T_{B,37V}$ (bottom) for frozen (blue) and thawed (red) training samples from the calibration stations.

TABLE 3

Classification accuracy of each land surface type.

Land surface type	Number of stations	SMMR accuracy (%)			SSM/I accuracy (%)		
		Freeze	Thaw	Total	Freeze	Thaw	Total
Irrigated cropland	5	82.3	90.8	89.3	80.2	95.9	89.8
Non-irrigated cropland	106	90.9	86.9	88.7	84.4	94.0	90.5
Dense forest	28	88.8	81.9	85.5	85.5	87.0	86.8
Shrub land	7	91.6	83.2	87.3	85.5	90.6	88.5
Sparse forest	11	91.3	86.7	89.1	81.6	89.4	88.4
Higher coverage grassland	38	85.7	87.1	87.1	80.6	93.9	86.1
Moderate coverage grassland	42	84.7	88.5	86.6	83.7	93.4	88.2
Lower coverage grassland	16	89.7	84.5	87.4	87.5	91.3	89.6
Unusable land	20	83.4	82.9	83.6	85.3	88.4	87.4
Total	273	88.3	86.2	87.4	84.0	92.4	88.7

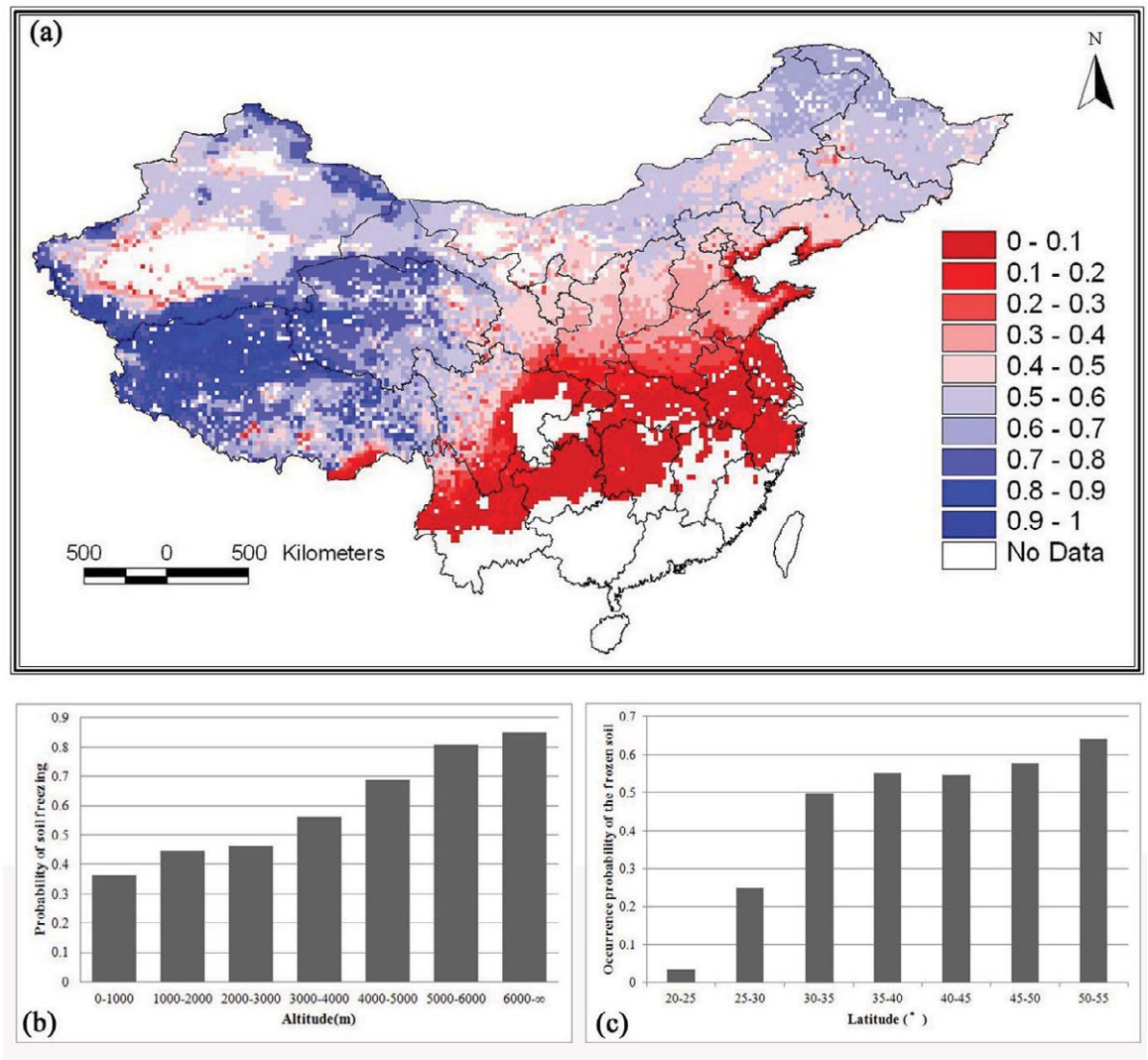

FIGURE 6. (a) Probability of soil freezing from 1978 to 2008 and (b) its variation with altitude and (c) latitude.

occurred in 1993/1994 when the frozen extent was 6.47×10^6 km^2 or 67.9%, and the coldest winter occurred in 2007/2008 when the frozen extent was 7.27×10^6 km^2 or 76.3%; this cold period resulted from a major snow and freezing-rain event in southern China.

TIMING AND DURATION OF SURFACE SOIL FREEZING

The first day of surface soil freezing is defined as the first day after 1 July that a grid is classified as being in a frozen state. Considering the average for the 30-year study period (see Fig. 9, part a), the first day of soil freezing occurred in July on the northwestern Qinghai-Tibetan Plateau, in August and September on the eastern portion of the Qinghai-Tibetan Plateau, in September and October in northeastern China, and in October and November in northern China. The standard deviations for the first day of soil freezing (see Fig. 9, part b) are one month in most regions of China, which means that the first day of soil freezing is relatively fixed. However, the standard deviation changes significantly as a result of short-time frozen ground caused by unusual cold currents in southern China. The pattern of the earliest first day of soil freezing (see Fig. 9, part c) is roughly similar to that of the average except for in northeastern China and southern China. The latest first days of soil freezing (see Fig. 9, part d) are generally one month after the average.

The last day of surface soil freezing is the last day before 30 June that a grid is classified as being in a frozen state. The average last day of soil freezing varies widely; it occurs in May or June on the Qinghai-Tibetan Plateau, in April in northwestern and northeastern China, in March in northern China, and in February or January in southern China (see Fig. 10, part a). The standard deviation is also steady at one month over most regions (see Fig. 10, part b). The earliest last day of soil freezing is advanced by approximately one month on the southeastern Qinghai-Tibetan Plateau and in northeastern and northwestern China (see Fig. 10, part c). The latest last day of soil freezing is delayed for one month in northeastern and southern China but does not change perceptibly in other regions of China (see Fig. 10, part d).

The duration of surface soil freezing is defined as the number of days between the first and last day of surface soil freezing, and the surface soil may periodically be thawed during this period. The northeastern Qinghai-Tibetan Plateau has the longest duration of surface soil freezing, above 300 days where permafrost is widely distributed, whereas the southern and eastern portions of Qinghai-

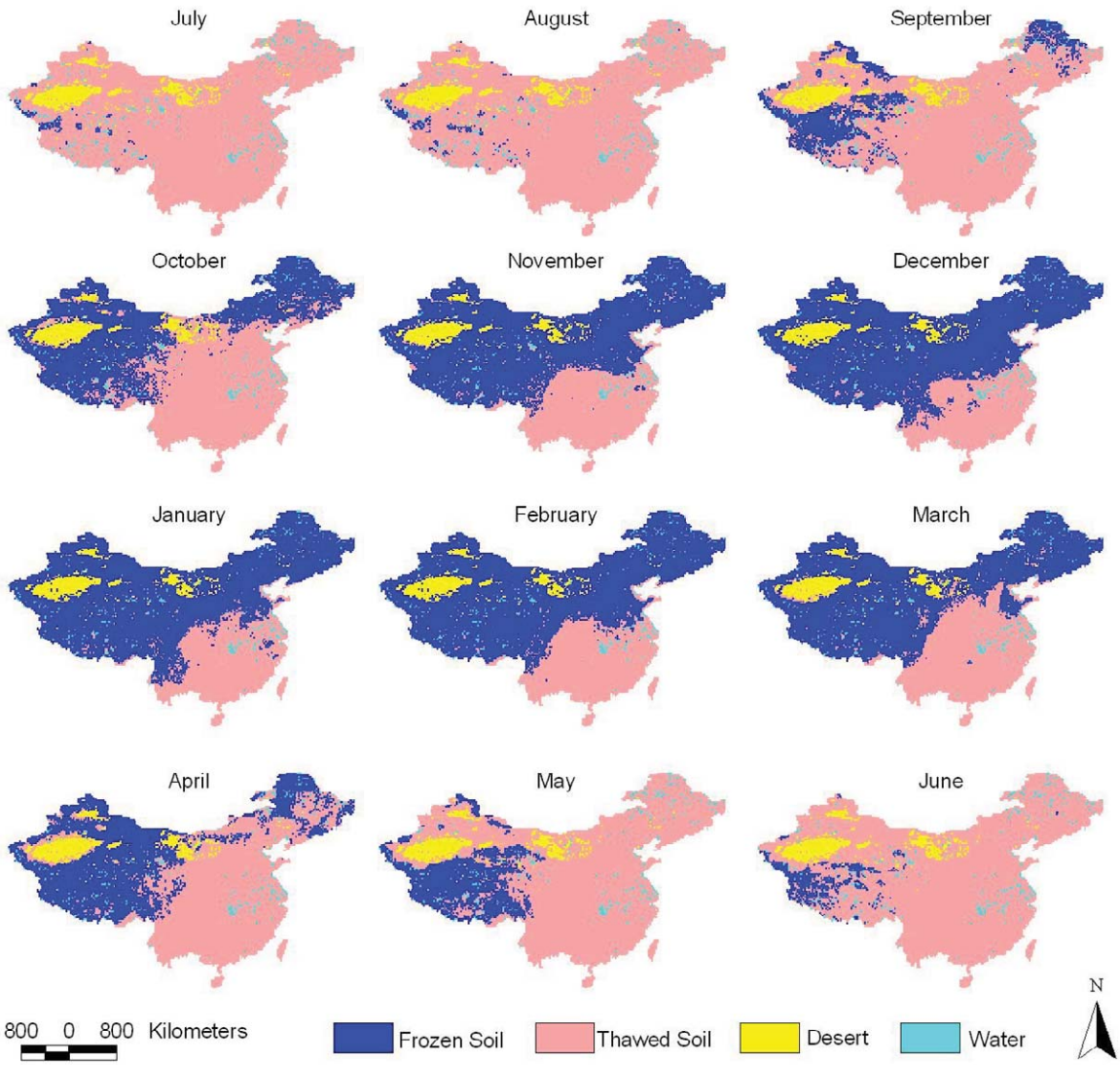

FIGURE 7. Monthly distribution of surface soil freeze-thaw status on the 15th day of each month from July 1, 2001, to June 30, 2002.

Tibetan Plateau remain in a frozen state for approximately 200–300 days. In other regions, the duration of surface soil freezing decreases with latitude; that is, it is greater than 150 days in northeastern China, approximately 120–180 days in northern China, and less than 60 days in southern China (see Fig. 11, part a).

The actual number of frozen days is considered to exclude the thawed period from the duration of surface soil freezing; both have a similar distribution pattern, but the former is generally shorter than the latter by 1–30 days (see Fig. 11, part b).

The frequency of soil freezing is the frequency of surface soil freeze-thaw cycles during an analysis year. On average, the Qinghai-Tibetan Plateau is frozen two to three times annually, northeastern and northern China are frozen one to two times annually, and southern China is frozen three times annually (see Fig. 11, part c).

TREND ANALYSIS

The long time-series data set provides an opportunity to analyze the timing of surface soil freeze-thaw cycles and the response of this cycle to climate change. The linear trends of the onset date of soil freezing and thawing and the duration of soil thawing across China have been detected for each pixel during 1978–2008.

The onset date of soil freezing is defined as the first day after 1 July that a grid is classified as being in a frozen state for three successive days. The onset date of soil thawing is defined as the first day before 1 July that a grid is identified as being in a thawed state for three successive days. The duration of soil thawing is defined as the number of days between the onset date of soil thawing and freezing. We assume that a stable and confident trend analysis would be obtained by using the definition of the onset dates of soil freezing and thawing because they exclude the influence of an occasional cold current on the first or last days of surface soil freezing.

In terms of trend analysis, linear least-square regressions are conducted for the above three indices. The statistical significance of any trend is verified by an F-test at a 90% confidence level, and only trends satisfying the F-test are accepted for further analysis and demonstration.

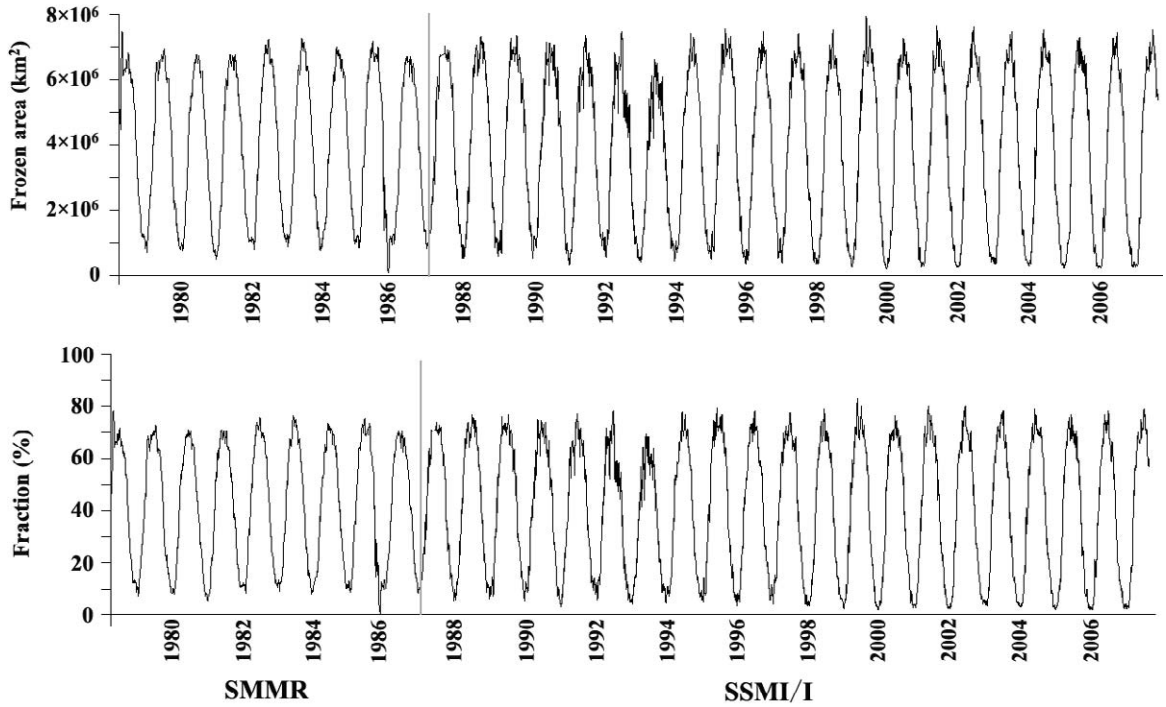

FIGURE 8. Daily total area of frozen soil over China from 1978 to 2008.

The onset date of soil freezing is postponed on average by 19.6 ± 14.6 days during 1978–2008 across China, by approximately 10 days in northeastern China, and by 30 days on the Tibetan Plateau (see Fig. 12, part a). There is no detectable trend in the northwestern part of the Tibetan Plateau because the permafrost there is stable. The onset date of soil thawing is advanced on average by 19.0 ± 9.4 days across China, particularly in the warm permafrost region and seasonally frozen ground region (see Fig. 12, part b). The duration of soil thawing is generally prolonged by approximately 32.5 ± 18.3 days and generally occurs in the warm permafrost and seasonally frozen ground regions (see Fig. 12, part c).

The above trend analysis reveals a pattern of earlier thawing, later freezing, and longer growing seasons as a result of climate warming. This pattern was also confirmed by the range of warming of air temperatures in China, which is approximately 0.5–0.8 °C 100 a^{-1}; in addition, one of the warming periods has occurred from 1980 to the present (Qin and Xiao, 2009) and is within the research period of this paper. Furthermore, climate warming and its influence on frozen ground are also demonstrated by observations of the in situ air temperature (Zuo et al., 2004), upper and lower limits of frozen soil (Gao et al., 2003), crop productivity (Wang et al., 2012), and cryosphere changes (Li et al., 2008; Kang et al., 2010). There is also positive feedback between the surface soil freeze/thaw cycles and climate change, which are illustrated by the enhanced heat exchange between the atmosphere and ground surface that likely enhance the plateau monsoons (Cheng and Wu, 2007) and release trapped carbon dioxide into the atmosphere at earlier times during thawing (Zhang, 2007).

Summary and Discussion

By combining the SMMR (1978–1987) and SSM/I (1987–2008) brightness temperature records, we have recalibrated the threshold of $T_{B.37V}$ in the dual-indices algorithm. As a result, a 30-year-long time-series data set of surface soil freeze-thaw states was produced and used in an analysis of the extent, timing, and trend of surface soil freeze-thaw cycles.

Two improvements distinguish this work from previous research. First, the threshold is determined for each land surface type as opposed to using a uniform value throughout the research region. This approach allows us to consider land type heterogeneity and improve the classification accuracy. Second, in situ daily minimum surface temperatures are used to calibrate the dual-indices algorithm, ensuring its ability to accurately capture the daily surface soil freeze-thaw cycle.

The above improvements yielded classification accuracies of approximately 88.3% for the frozen soil when using the SMMR and 84.0% when using the SSM/I, and classification accuracies of 86.2% for the thawed soil when using the SMMR and 92.4% when using the SSM/I. The total classification accuracy is approximately 87.4% for SMMR and 88.7% for SSM/I.

The analysis of extent and timing of surface soil freeze-thaw cycles demonstrated the following: (1) The maximum frozen extent during 1978–1987 was 6.93×10^6 km^2, or a 72.8% areal fraction, and it generally occurred in late December and January. The minimum frozen extent was 0.26×10^6 km^2, or a 3.0% areal fraction, and it occurred in late July and August. (2) The timing of the surface soil freeze/thaw cycles varies widely across China and is primarily dependent on the altitude and latitude. Generally, the first day of soil freezing occurs during September and November, the first day of soil thawing is between March and May, the duration of surface soil freezing is between 0 and 365 days, and the frequency of soil freezing is approximately one to three times annually.

The trend analysis revealed that the onset date of soil freezing is postponed on average by 19.6 ± 14.6 days across China and onset date of soil thawing is advanced on average by 19.0 ± 9.4 days.

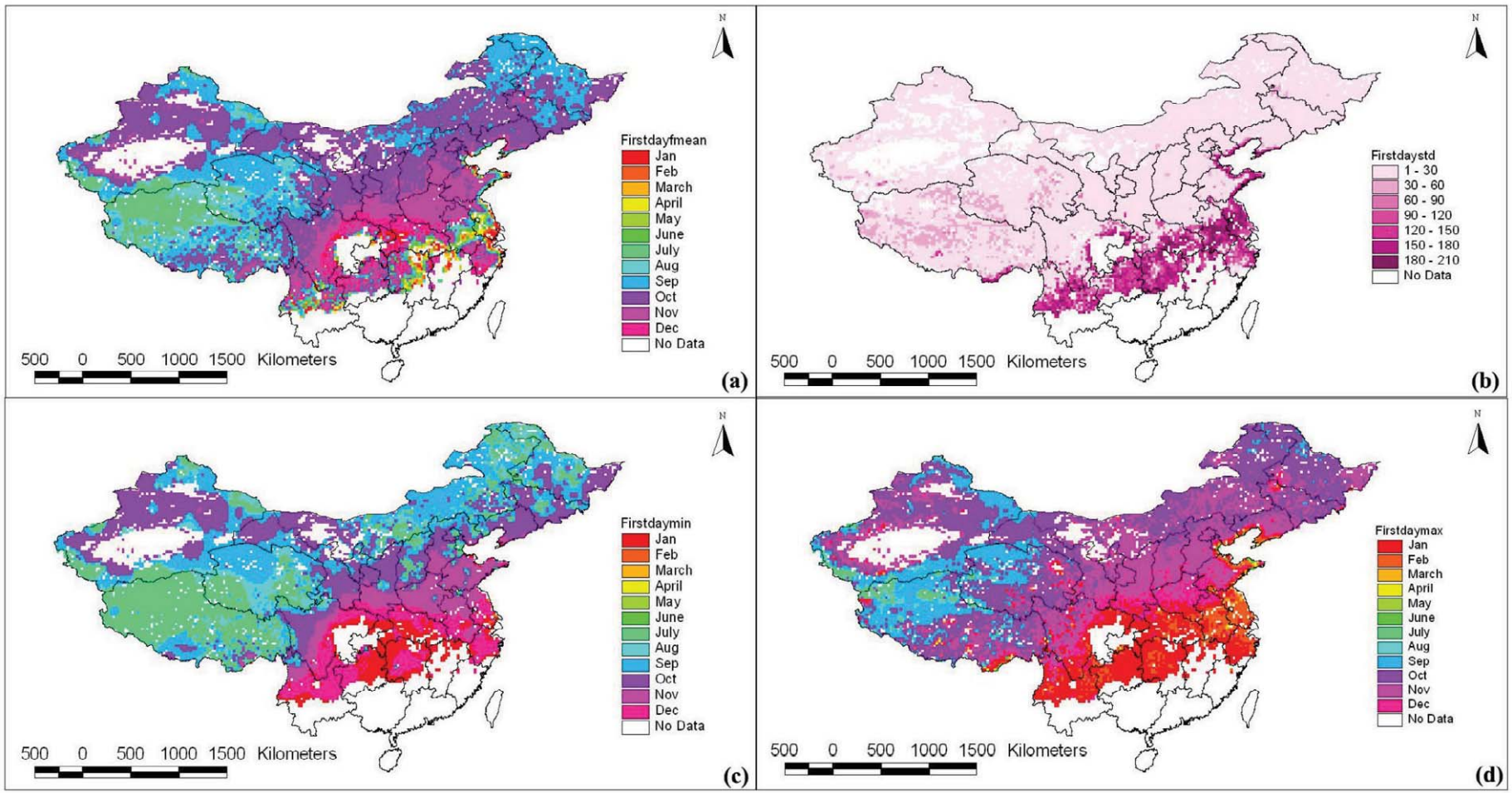

FIGURE 9. (a) Mean, (b) one standard deviation, (c) earliest date, and (d) latest date of the first day of soil freezing for 30 years (1978–2008).

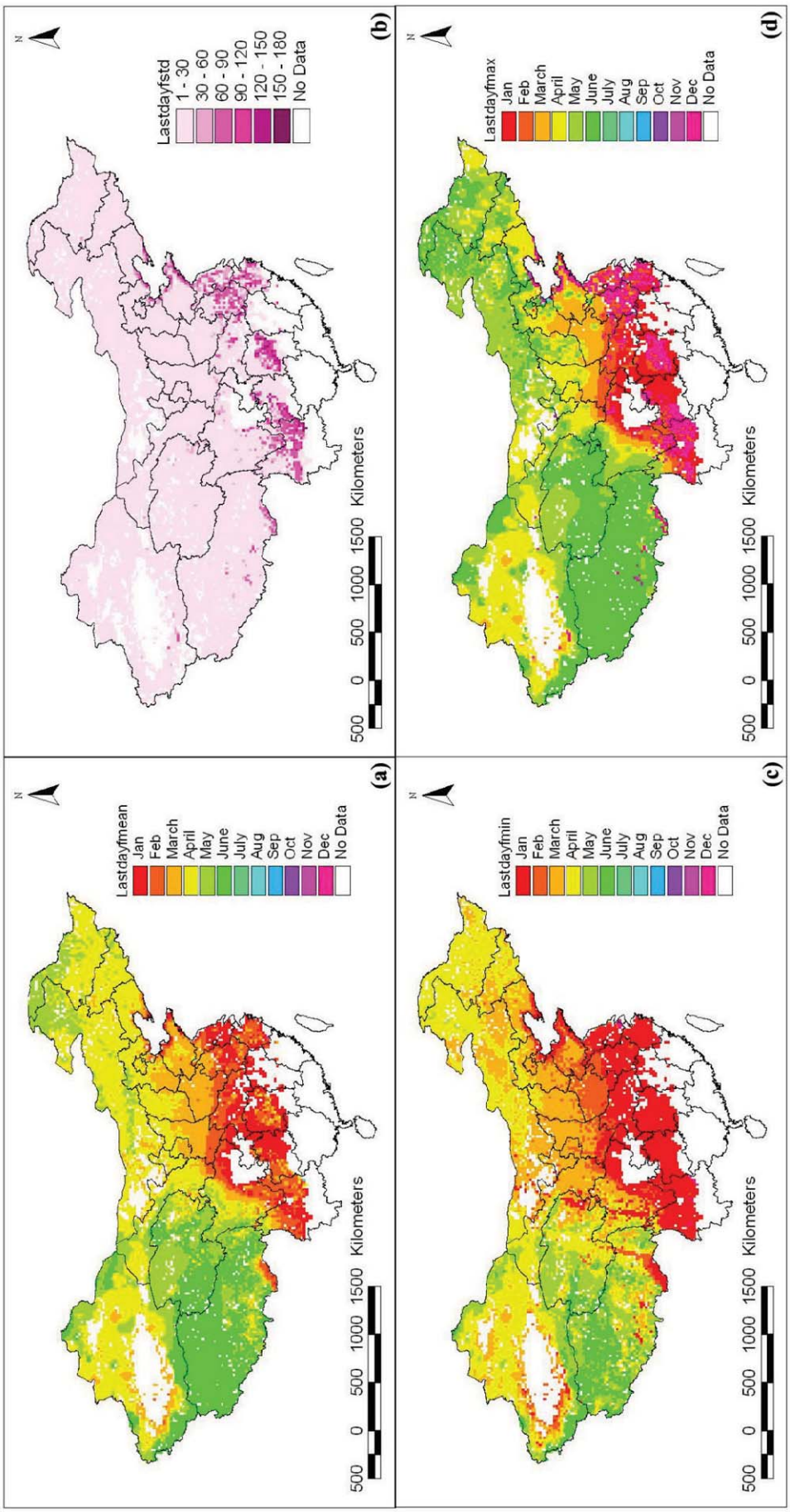

FIGURE 10. (a) Mean, (b) one standard deviation, (c) earliest date, and (d) latest date of the last day of soil freezing for 30 years (1978–2008).

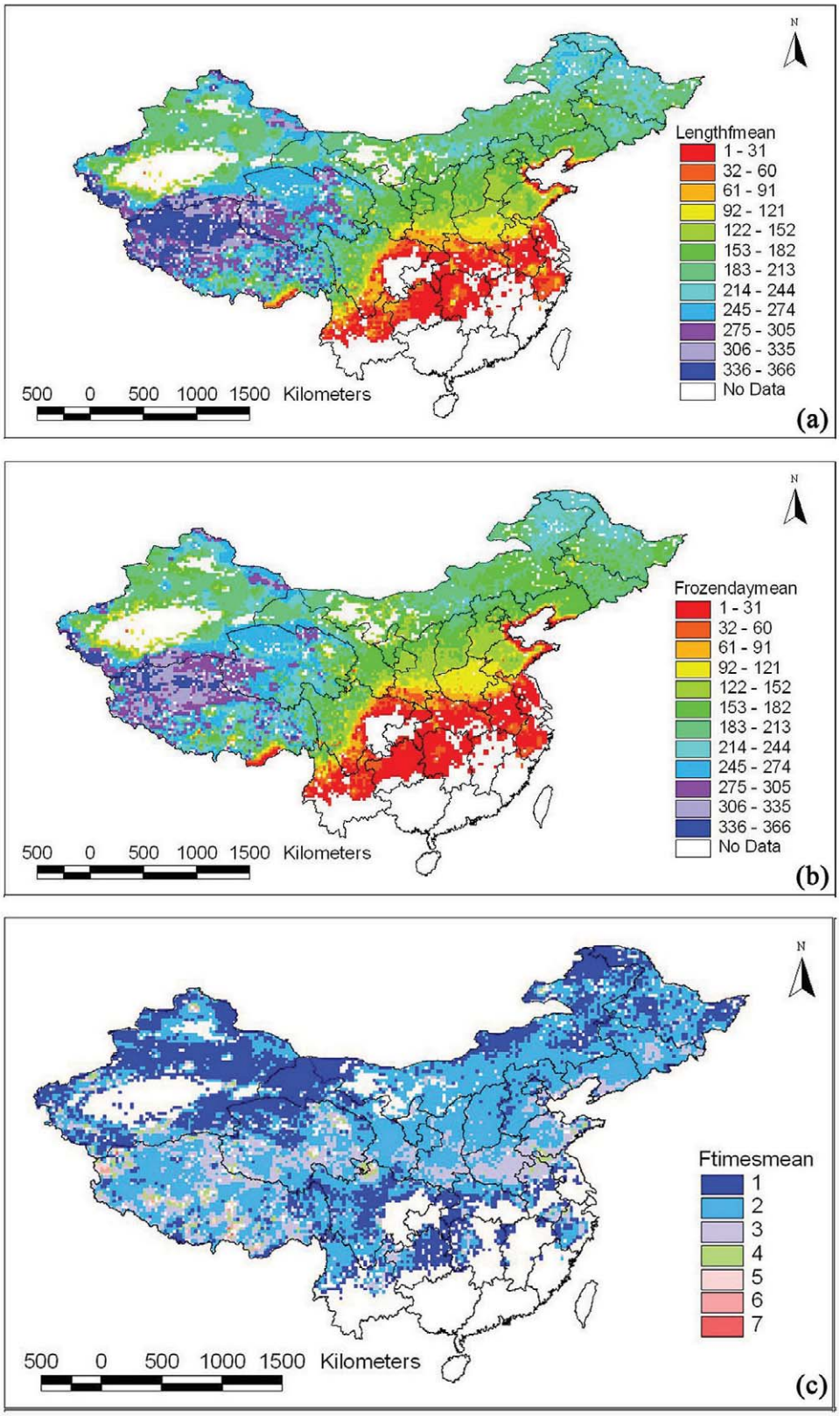

FIGURE 11. (a) Mean duration of soil freezing, (b) actual number of frozen days, and (c) frequency of soil freezing for 30 years (1978–2008).

Both changes result in the general prolonging of the soil thawing period by approximately 32.5 ± 18.3 days. These changes generally correspond to climate warming.

Compared with the results of sporadic observations, the surface soil freeze-thaw cycle data set obtained through the application of long-term global remote sensing observations can help us to deter-

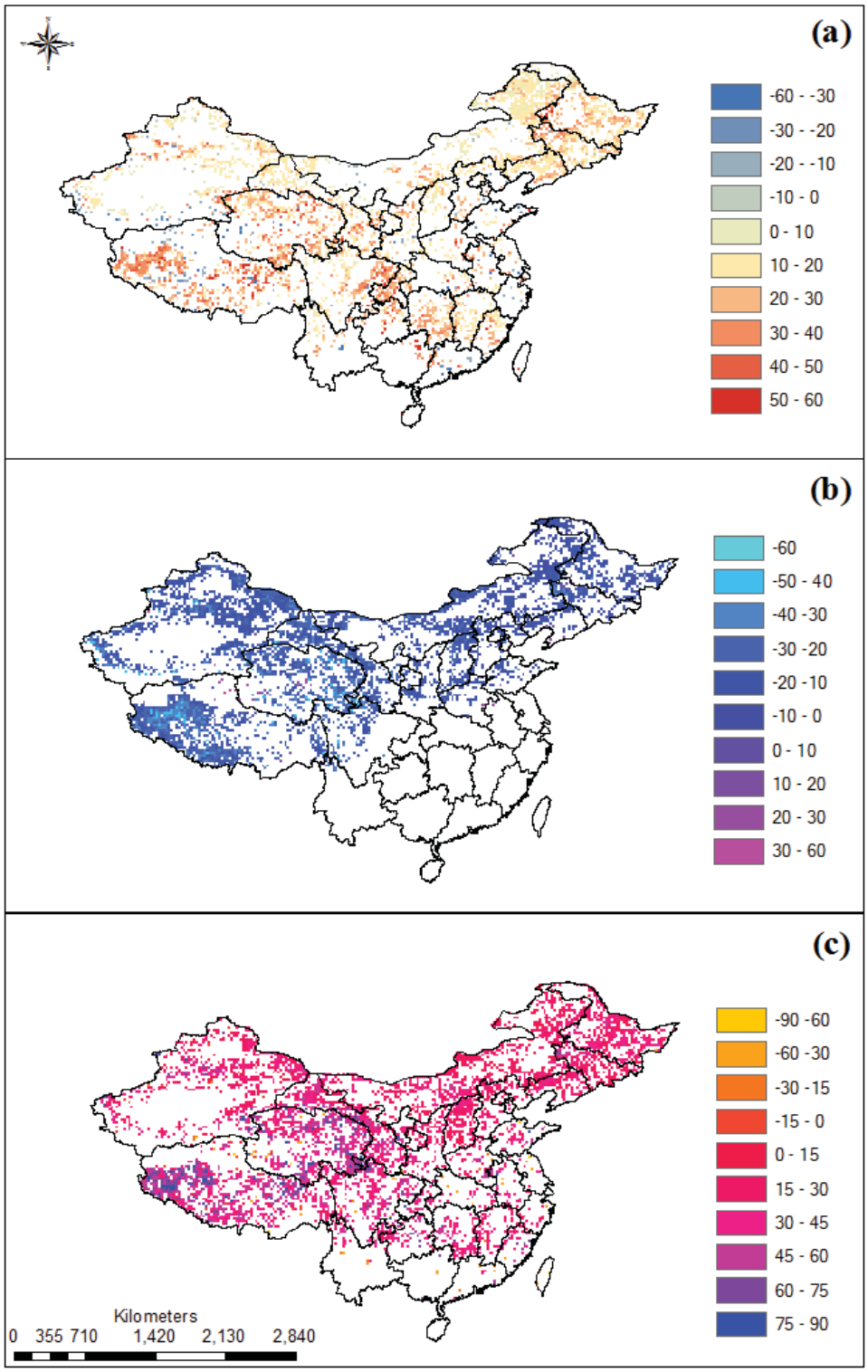

FIGURE 12. Trend of (a) onset date of soil freezing, (b) onset date of soil thawing, and (c) duration of soil thawing during 1978–2008 (unit: days).

mine changes in frozen ground at a regional scale. This data set will be updated and extended in the near future by using the multi-source remote sensing data and information fusion method. For example, NSIDC has published a co-registered AMSR-E (Advanced Microwave Scanning Radiometer for EOS), QuikSCAT (Quick Scatterometer), and WMO (World Meteorological Organization) Dataset (Tedesco and Miller, 2010) to provide additional information on the combination of active and passive microwave data for the extraction of geophysical parameters. Additionally, the SMAP (Soil Moisture Active and Passive) satellite, launched in 2015, will use the synchronous L-band SAR (Synthetic Aperature Radar) and radiometer data to detect the surface soil freeze-thaw cycle and provide a daily soil freeze-thaw data set with 3 km spatial resolution and 80% accuracy (Entekhabi et al., 2004; Bindlish et al., 2009). Combining active and

passive remote sensing is expected to improve the classification of surface soil freeze-thaw states by fusing brightness temperatures and backscattering information and increase the temporal resolution required to identify the daily surface soil freeze-thaw cycle by using multi-overpass observations from multi-sensors.

However, wavelength limitations only allow microwave sensing to provide surface soil freeze-thaw state information at a depth of 0–10 cm when using SMMR and SSM/I. Although the L-band microwave radiometer can penetrate frozen soil to a depth of 1 m, it is difficult to directly correlate soil freeze-thaw states with permafrost distribution. The in-depth analysis of the relationship between the surface soil freeze-thaw cycle and frozen ground distribution should be supported through the combination of a frozen soil model, data assimilation methods, field surveys, and long-term in situ observations.

Acknowledgments

This work was supported by the National Natural Science Foundation of China (91225302, 91125001, 41471357). We are grateful for the EASE-Grid SMMR and SSM/I brightness temperature data sets that were generously provided by the National Snow and Ice Data Center of the University of Colorado and in situ surface temperature observations that were provided by the CMA and CEOP project.

References Cited

Armstrong, R. L., Knowles, K. W., Brodzik, M. J., and Hardman, M. A., 2008: DMSP SSM/I Pathfinder daily EASE-Grid brightness temperatures. Boulder, Colorado: National Snow and Ice Data Center. Digital media.

Bartsch, A., Kidd, R. A., Wagner, W., and Bartalis, Z., 2007: Temporal and spatial variability of the beginning and end of daily spring freeze/thaw cycles derived from scatterometer data. *Remote Sensing of Environment*, 106(3): 360–374.

Basist, A., Grody, N. C., Peterson, T. C., and Williams, C., 1998: Using the special sensor microwave/imager to monitor land surface temperatures, wetness and snowcover. *Journal of Applied Meteorology*, 37: 888–911.

Bindlish, R., Jackson, T., Sun, R., Cosh, M., Yueh, S., and Dinardo, S., 2009: Combined passive and active microwave observations of soil moisture during CLASIC. *IEEE Transactions on Geoscience and Remote Sensing*, 6(4): 644–1274.

Black, T. A., Chen, W. J., Barr, A. G., Arain, M. A., Chen, Z., Nesic, Z., Hogg, E. H., Neumann, H. H., and Yang, P. C., 2000: Increased carbon sequestration by a boreal deciduous forest in years with a warm spring. *Geophysical Research Letter*, 27(9): 1271–1274.

Cheng, G. D., and Wu, T. H., 2007: Responses of permafrost to climate change and their environmental significance, Qinghai-Tibet Plateau. *Journal of Geophysical Research–Earth Surface,* 112(F2), http://dx.doi.org/10.1029/2006JF000631.

Derksen, C., and Walker, A. E., 2003: Identification of systematic bias in the cross-platform (SMMR and SSM/I) EASE-Grid brightness temperature time series. *IEEE Transactions on Geoscience and Remote Sensing*, 41(4): 910–915.

Entekhabi, D., Njoku, E. G., Houser, P., Spencer, M., Doiron, T., Kim, Y., Smith, J., Girard, R., Belair, S., Crow, W., Jackson, T. J., Kerr, Y. H., Kimball, J. S., Koster, R., McDonald, K. C., and Neill, P. E. O., 2004: The hydrosphere state (Hydros) satellite mission: an earth system pathfinder for global mapping of soil moisture and land freeze/thaw. *IEEE Transactions on Geoscience and Remote Sensing*, 42: 2184–2195.

Fiore, J. V., and Grody, N. C., 1992: Classification of snow cover and precipitation using SSM/I measurement: case studies. *International Journal of Remote Sensing*, 13(17): 3349–3361.

Frolking, S., McDonald, K. C., Kimbal, J. S., Way, J. B., Zimmermann, R., and Running, S. W., 1999: Using the space-borne NASA scatterometer (NSCAT) to determine the frozen and thawed seasons. *Journal of Geophysical Research*, 104(D22): 27895–27907.

Gao, R., Wei, Z. G., and Dong, W. J., 2003: Interannual variation of the beginning date and the ending date of soil freezing in the Tibetan plateau. *Journal of Glaciology and Geocryology*, 25(1): 49–54.

Goulden, M. L., Wofsy, S. C., Harden, J. W., Trumbore, S. E., Crill, P. M., Gower, S. T., Fries, T., Daube, B. C., Fan, S. M., Sutton, D. J., Bazzaz, A., and Munger, J. W., 1998: Sensitivity of boreal forest carbon balance to soil thaw. *Science*, 279(9): 214–217.

Grody, N. C., 1991: Classification of snow cover and precipitation using the special sensor microwave imager. *Journal of Geophysical Research*, 96(D4): 7423–7435.

Jarvis, P., and Linder, S., 2000: Constraints to growth of boreal forests. *Nature*, 405: 904–905.

Jin, R., Li, X., and Che, T., 2009: A decision tree algorithm for surface freeze/thaw classification using SSM/I. *Remote Sensing of Environment*, 113: 2651–2660.

Judge, J., Galantowicz, J. F., England, A. W., and Dahl, P., 1997: Freeze/thaw classification for prairie soils using SSM/I radiobrightnesses. *IEEE Transactions on Geoscience and Remote Sensing*, 35(4): 827–832.

Kang, S. C., Xu, Y. W., You, Q. L., Flügel Wolfgang-Albert, Pepin, N., and Yao, T. D., 2010: Review of climate and cryospheric change in the Tibetan Plateau. *Environmental Research Letters,* 5: 015101, http://dx.doi.org/10.1088/1748-9326/5/1/015101.

Kimball, J. S., McDonald, K. C., Frolking, S., and Running, S. W., 2004a: Radar remote sensing of the spring thaw transition across a boreal landscape. *Remote Sensing of Environment*, 89: 163–175.

Kimball, J. S., McDonald, K. C., Running, S. W., and Frolking, S. E., 2004b: Satellite radar remote sensing of seasonal growing seasons for boreal and subalpine evergreen forests. *Remote Sensing of Environment*, 90: 243–258.

Li, X., Cheng, G. D., Jin, H. J., Kang, E., Che, T., Jin, R., Wu, L. Z., Nan, Z. T., Wang, J., and Shen, Y. P., 2008: Cryospheric change in China. *Global and Planetary Change*, 62(3-4): 210–218

Liu, J. Y., Liu, M. L., Zhuang, D. F., Zhang, Z. X., and Deng, X. Z., 2003: Study on spatial pattern of land-use change in China during 1995–2000. *Science in China Series D: Earth Sciences*, 46(4): 373–384.

Mcdonald, K., and Kimball, J. S., 2005: Hydrological application of remote sensing: estimation of surface freeze-thaw states using microwave sensors. *In* Anderson, M. G., and McDonnell, J. J. (eds.), *Encyclopedia of Hydrological Sciences*, vol. 5. New York: John Wiley & Sons.

Picard, G., and Fily, M., 2006: Surface melting observations in Antarctica by microwave radiometers: correcting 26-year time series from changes in acquisition hours. *Remote Sensing of Environment*, 104: 325–336.

Qin, D., and Xiao, C., 2009: Global climate change and cryospheric evolution in China. *The European Physical Journal Conferences,* 1: 19–28.

Running, S., Way, J. B., McDonald, K. C., Kimball, J., and Frolking, S., 1999: Radar remote sensing proposed for monitoring freeze/thaw transitions in boreal regions. *Eos (Transactions, American Geophysical Union),* 80(19): 220–221.

Smith, N. V., Saatchi, S. S., and Randerson, J. T., 2004: Trends in high northern latitude soil freeze and thaw cycles from 1988 to 2002. *Journal of Geophysical Research*, 109: D12101, http://dx.doi.org/10.1029/2003JD004472.

Tedesco, M., and Miller, J., 2010: Co-registered AMSR-E, QuikSCAT, and WMO data. Boulder, Colorado: National Snow and Ice Data Center. Digital media.

Wang, J., Wang, E. L.,Yang, X. G., Zhang, F. S., and Yin, H., 2012: Increased yield potential of wheat-maize cropping system in the north China plain by climate change adaptation. *Climate Change*, 113(3-4): 825–840.

Wismann, V., 2000: Monitoring of seasonal thawing in Siberia with ERS scatterometer data. *IEEE Transactions on Geoscience and Remote Sensing*, 38(4): 1804–1809.

Zhang, T., 2007: Perspectives on environmental study of response to climatic and land cover/land use change over the Qinghai-Tibetan plateau: an introduction. *Arctic, Antarctic, and Alpine Research,* 39(4): 631–634.

Zhang, T., and Armstrong, R. L., 2001: Soil freeze/thaw cycles over snow-free land detected by passive microwave remote sensing. *Geophysical Research Letters*, 28(5): 763–766.

Zhang, T., Armstrong, R. L., and Smith, J., 2003: Investigation of the near-surface soil freeze-thaw cycle in the contiguous United States: algorithm development and validation. *Journal of Geophysical Research*, 108(D22): 8860, http://dx.doi.org/10.1029/2003JD003530.

Zuerndorfer, B., and England, A. W., 1992: Radiobrightnesses decision criteria for freeze/thaw boundaries. *IEEE Transactions on Geoscience and Remote Sensing*, 30(1): 89–102.

Zuerndorfer, B., England, A. W., Dobson, M. C., and Ulaby, F. T., 1990: Mapping freezing/thaw boundary with SMMR data. *Agricultural and Meteorology*, 52: 199–225.

Zhou, Y. W., Guo, D. X., Qiu, G. Q., Cheng, G. D., and Li, S. D., 2000: *Geocryology in China*. Beijing: Science Press, 450 pp. (in Chinese).

Zuo, H. C., Lv, S. H., and Hu, Y. Q., 2004: Variations trend of yearly mean air temperature and precipitation in China in the last 50 years. *Plateau Meteorology,* 23(2): 238–244.

MS accepted October 2014